BNL-69467

KINETIC EXTENSIONS OF THE NUCLEATION THEOREM

Robert McGraw
Atmospheric Sciences Division
Environmental Sciences Department
Brookhaven National Laboratory
Upton, NY 11973-5000

David T. Wu
Department of Mechanical Engineering
Yale University
New Haven, CT 06520

November 2002

Submitted to
J. Chem. Phys.

Research by BNL investigators was performed under the auspices of the U.S. Department of Energy under Contract No. DE-AC02-98CH10886.

ABSTRACT

Kinetic extensions of the nucleation theorem (KNT) are derived using the law of mass action and detailed balance. Results are obtained for the first and higher-order derivatives of the nucleation rate, *J*, with change in supersaturation, *S*, in terms of the cumulants, κ_n, of a molecular distribution of reciprocal equilibrium cluster growth rates. At constant temperature we find $d \ln J / d \ln S = \kappa_1 + 1$, an exact formulation of the nucleation theorem in terms of nucleation rate, and the extension $d^n \ln J / d(\ln S)^n = (-1)^{n+1} \kappa_n$ for the higher-order derivatives $(n \geq 2)$. The case $n = 2$ is related to the Kelvin relation. Analysis of recent water vapor nucleation rates [Wölk and Strey, J. Phys. Chem. B105, 11683, (2001)] provides molecular-based estimates for κ_1 and κ_2 suitable for comparison with the predictions of classical nucleation theory. The KNT is applied to ion-induced nucleation from the gas phase, by a sequence of reversible chemical reactions, and extensions to multi-step kinetics and multi-component nucleation are presented. Nucleation theorems enable one to deduce molecular-level properties directly from macroscopic rate measurements. Here we show these properties are not those of a single cluster, the critical nucleus, as approximate forms of the theorems would suggest, but instead are averages over a weighted distribution of clusters near critical size.

1. INTRODUCTION

A very useful result that has come to be called the 'nucleation theorem' is the following relationship between the height of the barrier to nucleation, W^*, and the nucleus size [1,2]

$$\left(\frac{\partial W^*}{\partial \Delta\mu}\right)_T = \left(\frac{\partial W^*/kT}{\partial \ln S}\right)_T = -\Delta g^*. \qquad (1.1a)$$

The derivative is taken at constant temperature and $\Delta g^* = g^* - n_v^*$ is the excess number of molecules in the critical cluster (g^* is the number of molecules in the cluster and n_v^* is the number of vapor molecules displaced by the cluster volume). S is the saturation ratio and $\Delta\mu = kT\ln S$ is the free energy difference between the vapor and the bulk condensed phase driving the phase change. For nucleation from a dilute vapor the displacement term is negligible and $\Delta g^* \approx g^*$.

The nucleation theorem, as given in Eq. 1.1a, is a thermodynamic relation that has been obtained on fundamental grounds by several approaches including a statistical mechanical derivation by Viisanen et al. [3,4] and a Gibbs dividing surface analysis by Oxtoby and Kashchiev [2]. In addition to aiding the interpretation of experimental measurements (see below), the nucleation theorem has been used as an analytical tool and guide for introducing a molecular basis to phenomenological nucleation theories [5]. Recent studies have focused on the range of validity of the nucleation theorem, on related equalities, and on applications to fields other than nucleation [6,7].

Nonisothermal versions of the nucleation theorem have also been investigated [2,8]. For the temperature derivative at constant $\ln S$, Ford gives the following result [8]:

$$\left(\frac{\partial W^*}{\partial T}\right)_{\ln S} = -\frac{E_{g^*} - g^* E_1^b}{kT^2} \qquad (1.1b)$$

where E_{g^*} is the critical cluster energy and E_1^b is the energy per molecule in the bulk liquid phase.

An obvious limitation of Eqs. 1.1 is that W^* and E_{g^*} are not directly observable quantities. Thus practical applications require going beyond Eqs. 1.1 in order to make contact with experimental measurements of the steady-state nucleation rate (J). Here the arguments have been less fundamental. The usual approach assumes that J has the prefactor-exponent form:

$$J = J_0 \exp(-W^*/kT) \tag{1.2}$$

where J_0 is the kinetic prefactor, k is the Boltzmann constant and T is absolute temperature. Combining Eqs. 1 and 2 gives the relative sensitivity of J to changes in S [9]:

$$\frac{S}{J}\frac{dJ}{dS} = \frac{d\ln J}{d\ln S} = \frac{d\ln J_0}{d\ln S} + \Delta g^*. \tag{1.3}$$

The lead term on the right-hand-side (rhs) is typically a small constant value or zero, depending on model. For classical nucleation theory (CNT) $d\ln J_0 / d\ln S = 2$. Taking into account the $1/S$ prefactor correction of Courtney [10] changes this to $d\ln J_0 / d\ln S = 1$ and Eq. 1.3 becomes [2]:

$$\frac{d\ln J}{d\ln S} = 1 + \Delta g^*. \tag{1.4}$$

A more complete expression for the left hand side of Eq. 1.4 was obtained by Ford [11] by differentiating the Becker-Doring expression for the nucleation rate. We refer to this new kind of result, which depends on the kinetics as well as on the thermodynamics of the nucleation process, as a kinetic nucleation theorem (KNT). Kinetic nucleation theorems predict change in the nucleation rate itself, rather than in the barrier height whose interpretation through experiment is at best indirect.

In this paper we obtain new KNTs for the higher-order derivatives, $d^n \ln J / d(\ln S)^n$, and apply these to the interpretation of recent measurements for the homogeneous nucleation rate of water vapor. Theoretical foundation for the KNT is presented in Sec. 2 based on the physio-chemical principles of mass action and detailed balance. Similar results are applied in Sec. 3 to nucleation from the gas phase by a reversible sequence of chemical reactions. These results show

that the isothermal rate sensitivity depends only on reaction stoichiometry and not on molecular bonding condition or location within the cluster. Section 4 initiates the extension of KNTs to multicomponent nucleation. Formulations of the theorem are obtained for binary nucleation in special systems, such as sulfuric acid-water mixtures, and for multicomponent systems having a quadratic free-energy surface. A matrix approach suitable for numerical calculation of the rate sensitivity for general multi-step and multi-component nucleation processes is also described. Section 5 gives a sumary and discussion of results. In particular, we conclude that measurements of $d^n \ln J / d(\ln S)^n$ provide direct molecular-level information, which is averaged over certain distributions of clusters near critical size and not specific to the critical cluster itself.

2 DERIVATION OF KINETIC NUCLEATION THEOREMS FROM THE LAW OF MASS ACTION AND DETAILED BALANCE

This section introduces a fundamental approach to evaluating the left hand side of Eq. 1.4 and higher-order derivatives, through application of the law of mass action and detailed balance. The approximations that underly Eq. 1.2 are bypassed and the evaluation of $d \ln J / d \ln S$ is carried out directly on the kinetic sequence of monomer addition/loss steps that govern the nucleation rate. Detailed balance is incorporated by working directly with the Becker-Doring summation for the steady state nucleation rate [12]:

$$J = \left(\sum_g \frac{1}{\beta_g n_g} \right)^{-1} = \left(\sum_g \frac{4}{c_1 s_g n_1 n_g} \right)^{-1} . \tag{2.1}$$

Here n_g is the constrained equilibrium concentration of clusters of size g (clusters containing g monomeric units) and β_g is the rate constant for monomer addition to clusters of this size:

$$\beta_g \equiv \frac{c_1}{4} s_g f_1 = \left(\frac{kT}{2\pi m_1} \right)^{1/2} s_g f_1 = \left(\frac{kT}{2\pi m_1} \right)^{1/2} s_g n_1 \tag{2.2}$$

where s_g is the surface area of a g-cluster and c_1 is the mean molecular speed of a molecule of mass m_1. The last equality uses the monomer boundary condition $f_1 / n_1 = 1$ [12] where n_1 and f_1 are the constrained equilibrium and actual concentrations of monomer in the vapor phase.

The constrained equilibrium concentrations, n_g (cm^{-3}), are related through the reversible chemistry $A_{g-1} + A_1 = A_g$ according to the law of mass action:

$$K_g^{eq}(T) = \frac{[A_g]}{[A_1][A_{g-1}]} \approx \frac{n_g}{n_1 n_{g-1}} \tag{2.3}$$

where A_g denotes a cluster containing g monomers, $[A_g]$ is the activity of these clusters and $K_g^{eq}(T)$ is a function of temperature alone [13]. The last equality, the law of mass action, applies to an ideal mixture of clusters for which activity is proportional to number concentration. The vapor phase monomer versus bulk free energy difference is

$$\Delta\mu = kT \ln S = kT \ln(n_1) - kT \ln(n_1^{eq}) \tag{2.4}$$

where S is the saturation ratio of monomer (A_1) and n_1^{eq} is the number concentration of monomer in equilibrium with the saturated liquid. The latter is constant at constant temperature, as we neglect any effect of pressure change on the vapor pressure of the bulk liquid. Equations 2.1-2.4 are sufficient to derive the kinetic extension of nucleation theorem. For obtaining the nucleation theorem from the equilibrium law of mass action, a key property of Eq. 2.3 is employed, specifically, that the population ratio, n_g / n_{g-1} is directly proportional to n_1. From this follows the proportionality $n_g \propto n_1^{\,g}$, yielding a convenient intermediate result for differentiating the product terms on the rhs of Eq. 2.1:

$$\frac{d(n_1 n_g)}{d \ln S} = (g+1) n_1 n_g . \tag{2.5}$$

2.1 Isothermal kinetics

The detailed balance condition for the reaction described by Eq. 2.3 gives a relation between the forward and reverse monomer addition in terms of the cluster population under constrained equilibrium conditions:

$$\beta_g n_g = \gamma_{g+1} n_{g+1} . \tag{2.6}$$

Together, the law of mass action and the detailed balance condition imply only that β_g / γ_{g+1} is proportional to n_1. Equation 2.2 implies a more specific kinetic model for which all of the

monomer dependence is in the condensation rate and the evaporation rate is independent of monomer concentration, a condition sufficient but not necessary for the law of mass action to apply. A KNT incorporating both detailed balance and mass action follows from Eqs. 2.1 and 2.5. On using the chain rule for differentiation of Eq. 2.1 at constant temperature, the result is:

$$\frac{d\ln J}{d\ln S} = 1 + \bar{g} \cong 1 + g^* \tag{2.7}$$

where the over bar signifies the following cluster-average with respect to the distribution $1/(\beta_g n_g)$

$$\bar{y} \equiv \frac{\sum_g \frac{1}{\beta_g n_g} y(g)}{\sum_g \frac{1}{\beta_g n_g}} = \sum_g P(g) y(g). \tag{2.8}$$

The last equality defines the normalized $1/(\beta_g n_g)$ distribution, $P(g)$. The present derivation applies to cluster formation from a dilute vapor and/or solute for which, as in the derivation of Eq. 2.1, the subtraction of displaced monomer can be neglected. Equations 2.7 and 2.8 are the more complete expressions for the lhs of Eq. 1.4 obtained by Ford [11].

Higher order derivatives can also be obtained and may be expressed remarkably simply in terms of the cumulants κ_n of $P(g)$. Together with the previous results from above these are (see Appendix):

$$\begin{aligned} \frac{d\ln J}{d\ln S} &= \bar{g} + 1 = \kappa_1 + 1 \\ \frac{d^2\ln J}{d(\ln S)^2} &= -(\overline{g^2} - \bar{g}^2) = -\kappa_2 \\ \frac{d^3\ln J}{d(\ln S)^3} &= \kappa_3 \end{aligned} \tag{2.9a}$$

$$\frac{d^4 \ln J}{d(\ln S)^4} = -\kappa_4$$
$$\vdots$$
$$\frac{d^n \ln J}{d(\ln S)^n} = (-1)^{n+1}\kappa_n$$

Equations 2.9a have a structure that arises not only from the statistical properties of cumulants, although these play an important role, but from the physio-chemical properties of cluster equilibria and kinetics embodied in the laws of mass action and detailed balance (see for example Eq. A1). The second of Eqs. 2.9a, or its equivalent relation $d\kappa_1 / d\ln S = -\kappa_2$ from Eq. A6, implies that the curvature on a plot of $\ln J$ vs $\ln S$ also has a direct interpretation in terms of molecular properties, specifically in terms of the variance of the $1/(\beta_g n_g)$ distribution. The frequent observation that plots of $\ln J$ vs $\ln S_1$ tend to be nearly linear is see here as a consequence of a narrow $1/(\beta_g n_g)$ distribution. For a continuous Gaussian distribution, the cumulants will vanish for index $n > 2$ [14] resulting in early termination of Eqs. 2.9 and a $\ln J$ that is quadratic in $\ln S$. Rooted in mass action and detailed balance, these results have general validity independent of any cluster model.

An application of Eqs. 2.9a to the interpretation of recent rate measurements for the homogeneous nucleation of water vapor is shown in Fig. 1. The data points are the reported nucleation rates for H_2O at $T = 250K$ from Table 2 of Wölk and Strey [15]. Equations 2.9a suggest a fit using a Taylor expansion of the form:

$$Log_{10}(J) = Log_{10}(J_0) + (\bar{g}+1)_{S_0} Log_{10}\left(\frac{S}{S_0}\right) - \frac{1}{2}(\kappa_2)_{S_0}\left[Log_{10}\left(\frac{S}{S_0}\right)\right]^2 + \cdots \qquad (2.9b)$$

where the switch to common logarithms for both $\ln J$ and $\ln S$ leaves Eqs. 2.9a unchanged. The solid curve in the figure is a quadratic fit to the data in powers of $Log_{10}S$ yielding $\bar{g}+1 = 30.86$

and $\kappa_2 = \overline{g^2} - (\bar{g})^2 = 49.42$ evaluated at the reference supersaturation $S_0 = 10$ (gray vertical line). This same fit yields the value $Log_{10}(J_0) = 8.762$(gray horizontal line). The dashed line shows the result of cutting off the Taylor expansion after the linear term whereas the solid curve uses both the linear and quadratic terms, showing the effect of curvature.

It is useful to compare these parameters, derived from measurement, with the expected results from classical nucleation theory. The top panel of Fig. 2 shows the classical barrier profile, $W_{CNT}(g)/kT = -g\ln S + \alpha g^{2/3}/kT$, for homogeneous nucleation of water vapor under the conditions $S = 10$ and $T = 250K$, corresponding to the reference conditions used in Fig. 1. Here $\alpha = (4\pi)^{1/3}(3/\rho_l)^{2/3}\gamma_\infty$ where γ_∞ is the surface tension for a flat interface and ρ_l is the molecular number density in the bulk condensed phase. The CNT barrier calculation of Fig. 2 uses the same physiochemical properties for H_2O as in Wölk and Strey [15]. A good indication of $P(g)$, the cumulants of which are related to the observable sensitivities $d^n \ln J / d(\ln S)^n$ through Eqs. 2.9, can be had by inspecting its CNT-approximate form , $P_{CNT}(g)$, under these typical nucleation conditions. This is indicated by the solid curve in the lower panel of the figure. The width of this distribution is, from Eqs. 2.7 and 2.8, an indication of the extent to which measurements of $d^n \ln J / d(\ln S)^n$ yield weighted-average properties over many near-critical clusters, and are not specific to the critical cluster itself. The CNT calculations yield $g^*(CNT) = 30$ (nearest integer) and the moments: $\bar{g}(CNT) = 29.96$; $\kappa_2(CNT) = 39.04$. The classical $\bar{g}(CNT) + 1 = 30.96$ is in remarkably good agreement with the determination, $\bar{g} + 1 = 30.86$, from the experimental fit. The CNT prediction for κ_2 is lower than the experimental determination (see caption) by about 20%; however data scatter and strong background linearity on the experimental log-log plot makes this parameter inherently more difficult to estimate. Nevertheless the sign of the curvature (which from Eq. 2.9a must be negative) is correct, and its magnitude in rough agreement with the

prediction of classical nucleation theory. Equations 2.9 provide information on the general shape of the log-log rate plots, seen here to be in very good agreement with the predictions of CNT, but not on their displacement, or absolute value of the nucleation rate. Application of the Becker-Doring summation (Eq. 2.1) gives $Log_{10} J_0(CNT) = 9.49$, yielding a predicted nucleation rate about a factor of five higher than the experimental value, in agreement with the finding of Wölk and Strey [15].

The second equality of Eqs. 2.9a is closely related to the Kelvin relation, giving as it does the change in critical cluster size with supersaturation:

$$\frac{d\bar{g}}{d\ln S} = -(\overline{g^2} - \bar{g}^2) \approx \frac{dg^*}{d\ln S} \; . \tag{2.10}$$

To move closer to the spirit of the Kelvin relation, which is a thermodynamic result, we take averages in terms of the $1/n_g$ distribution (i.e. without the kinetic part, β_g, which cancels if assumed *g*-independent in the region of critical cluster size) and find a similar exact result: $d < g > / d\ln S = -(< g^2 > - < g >^2)$. The angular brackets are averages with respect to the normalized $1/n_g$ distribution, shown in the lower panel of Fig. 2 (dotted curve), which is only slightly shifted from $P_{CNT}(g)$. The classical Kelvin relation for the critical nucleus size is: $g^* = (8/27)\alpha^3 (kT \ln S)^{-3}$. Thus the change in nucleus size with supersaturation is:

$$\frac{dg^*}{d\ln S} = -\frac{8}{9}(\alpha / kT)^3 (\ln S)^{-4}. \tag{2.11}$$

The connection to the general result, Eq. 2.10, follows a demonstration that the negative variance of the $1/n_g$ distribution, as obtained from the capillary drop model distribution of the classical theory, is identical to the right hand side (of Eq. 2.11). Here $n_g \propto \exp\left(-g\ln S + \alpha g^{2/3}/kT\right) \equiv$

$\exp[-W_{CNT}(g)/kT]$. Expanding the exponent in a Taylor series through the quadratic term about g^* gives:

$$\frac{W_{CNT}(g)}{kT} \approx \frac{W_{CNT}(g^*)}{kT} - \frac{9}{16}\left(\frac{kT}{\alpha}\right)^3 (\ln S)^4 (g-g^*)^2. \qquad (2.12)$$

Equation 2.12 yields a Gaussian distribution for $1/n_g$ with $< g >= g^*$ and variance $\sigma^2 = (8/9)(\alpha/kT)^3(\ln S)^{-4} = -dg^*/d\ln S$, where the last equality is Eq. 2.11. This demonstrates the reduction of Eq. 2.10 to the classical Kelvin relation for the capillarity drop approximation of classical nucleation theory.

2.2 Temperature variation

Next we obtain the weighted cluster energy distribution appearing in an exact expression for the temperature dependence of the nucleation rate. Taking the temperature derivative of $\ln J$ from Eq. 2.1 gives:

$$\frac{d\ln J}{dT} = \overline{\frac{d\ln\{c_1 s_g n_1 n_g/4\}}{dT}} \qquad (2.13)$$

To evaluate the rhs of Eq. 2.13, we use

$$\frac{d\ln c_1}{dT} = \frac{1}{2T} \qquad (2.14)$$

from Eq. 2.2, and assume that the cluster surface area, s_g, is independent of T. This leaves only the derivative $d\ln(n_1 n_g)/dT$, which will now be evaluated using the Gibbs-Helmholtz relation [13].

Returning to Eq. 2.3, we form the equilibrium rate contant for the association of g monomers to form a molecular cluster of size g:

$$K(T) = K_g^{eq} K_{g-1}^{eq} \times \cdots \times K_2^{eq} = \frac{n_g}{n_1^g} \tag{2.15}$$

Applying the Gibbs-Helmholtz relation to the rhs, recalling that n_g has units of concentration, gives:

$$\frac{d \ln K(T)}{dT} = \frac{E_g - gE_1}{kT^2} \tag{2.16}$$

where E_g is cluster energy. Consider the following derivative with respect to temperature at constant S_1:

$$\left(\frac{\partial \ln n_1}{\partial T} \right)_{S_1} = \left(\frac{\partial \ln n_1^{eq}}{\partial T} \right)_{S_1} = \frac{d \ln n_1^{eq}}{dT} \tag{2.17}$$

where n_1^{eq} is the monomer concentration in the vapor at equilibrium over bulk liquid ($n_1 = n_1^{eq} S_1$). Similarly, from Eq. 2.15 and 2.17,

$$\left(\frac{\partial \ln n_g}{\partial T} \right)_{S_1} = \frac{d \ln n_g^{eq}}{dT} = \frac{d \ln K(T)}{dT} + g \frac{d \ln n_1^{eq}}{dT}. \tag{2.18}$$

The last term in Eqs. 2.18 is readily evaluated from the Clapeyron relation:

$$\frac{d \ln n_1^{eq}}{dT} = \frac{E_1 - E_1^b}{kT^2} \tag{2.19}$$

where E_1^b is the energy per molecule in the bulk liquid. Combining Eqs. 2.16, 2.17, and 2.19 gives the derivative that we have been seeking:

$$\left(\frac{\partial \ln(n_1 n_g)}{\partial T} \right)_{\ln S_1} = \frac{E_g - gE_1^b}{kT^2} + \frac{E_1 - E_1^b}{kT^2} \tag{2.20}$$

This expression together with Eqs. 2.13 and 2.14 gives the final result:

$$\left(\frac{\partial \ln J}{\partial T} \right)_{\ln S_1} = \frac{1}{2T} + \frac{\overline{E}_g - \overline{g} E_1^b}{kT^2} + \frac{E_1 - E_1^b}{kT^2} \tag{2.21}$$

where the overbar indicates averaging as in Eq. 2.8. The present derivation includes kinetics and shows explicitly the underlying physics as contained in the law of mass action, detailed balance, and the Gibbs-Helmholtz relation. Equation 2.21 differs from the thermodynamic result of Ford

[Eq. 48 of Ref. 11] by the leading term on the rhs (originating from Eq. 2.4), and by averging over $P(g)$, as signified here by the overbar, to rigorously include the kinetics contained in the Becker-Doring summation for J.

Equation 2.21 can be used to evaluate differences between the cluster energies inferred from experimental rate nucleation measurements and those obtained using the capillary drop model of CNT. Rewriting Eq. 2.21 for CNT and differencing gives:

$$\left(\frac{\partial \ln J/J_{CNT}}{\partial T}\right)_{\ln S_1} = \frac{\overline{E}_g - \overline{E}_g(CNT)}{kT^2} - \frac{[\overline{g} - \overline{g}(CNT)]E_1^b}{kT^2} \qquad (2.22)$$

Application of Eq. 2.22 is complicated by fact that the averages are over two different cluster distributions: the true molecular distribution $P(g)$, for $\overline{g}$ and $\overline{E}_g$, and the drop-model distribution $P_{CNT}(g)$ of CNT, for $\overline{g}(CNT)$ and $\overline{E}_g(CNT)$. On the other hand, there are widespread observations that the ratio J/J_{CNT} is a function of temperature alone (see for example [16]). Such observations imply that the Kelvin relation is satisfied and that the true nucleation barrier is uniformly shifted in energy from the CNT barrier by a temperature-dependent amount [5,17]. These properties greatly simplify the final result. Specifically, in the approximation that the barrier is uniformly shifted, the critical cluster size, the cluster ratios (n_g/n_{g*}), and $P(g)$ all have the same values as in CNT. Assuming identical molecular addition rates, β_g, and setting $P(g) = P_{CNT}(g)$, Eq. 2.22 simplifies to:

$$\frac{d\ln J/J_{CNT}}{dT} = \frac{\overline{E}_g - \overline{E}_g(CNT)}{kT^2} \approx \frac{E_{g*} - E_{g*}(CNT)}{kT^2} \qquad (2.23)$$

where the first equality holds for the case that J/J_{CNT} is a function of temperature alone. The weighting for both the molecular and CNT cluster energies in the numerator is the CNT distribution, $P_{CNT}(g)$. Measurements of J/J_{CNT} provide, through Eq. 2.23, direct information about the excess (with respect to CNT) cluster energies, which can be compared directly to phenomenological cluster models and calculations based on molecular theory.

3. APPLICATION TO NUCLEATION FROM THE GAS PHASE BY A REVERSIBLE SEQUENCE OF CHEMICAL REACTIONS

The kinetic nucleation theorem is next illustrated for a different kind of one-step process; one for which neither the kinetic prefactor nor the nucleation work are well defined. Consider nucleation from the gas phase by the reversible sequence of chemical reactions studied by Girshick [18]. This sequence is initiated by reaction of SiH_4 with the 'seed' ion SiH_3^-

$$SiH_3^- + SiH_4 = Si_2H_5^- + H_2 \tag{3.1a}$$

followed by growth steps:

$$\begin{aligned} Si_2H_5^- + SiH_4 &= Si_3H_7^- + H_2 \\ &\vdots \\ Si_{m-1}H_{2m-1}^- + SiH_4 &= Si_mH_{2m+1}^- + H_2 \end{aligned} \tag{3.1b}$$

leading to the formation of cluster ions of larger size. With the seed requirement, Eqs. 3.1 are formally equivalent to a heterogeneous or ion-induced nucleation process. Equation 2.3 is replaced by the equilibrium constant:

$$K_m(T) = \frac{[Si_mH_{2m+1}^-][H_2]^{m-1}}{[SiH_3^-][SiH_4]^{m-1}} \cong \frac{n(Si_mH_{2m+1}^-)\{n(H_2)\}^{m-1}}{n(SiH_3^-)\{n(SiH_4)\}^{m-1}} \tag{3.2}$$

where $[A]$ and $n(A)$ are the activity and number concentration, respectively, of species A under a (constrained) equilibrium condition. As with the monomer boundary condition used previously, $n(SiH_4)$, $n(H_2)$ and $n(SiH_3^-)$ are equated to the actual concentrations of these precursor species in the gas phase. Detailed balance considerations lead to an overall rate analogous to Eq. 2.1 [18]:

$$J = \left(\sum_m \frac{1}{k_m n(SiH_4) n(Si_mH_{2m+1}^-)} \right)^{-1} \tag{3.3}$$

where k_m is the forward bimolecular rate constant for the reaction of $Si_mH_{2m+1}^-$ with SiH_4. Differentiation of $\ln J$ is similar to derivation of Eq. 2.7. For brevity we give only the results:

$$\frac{\partial \ln J}{\partial \ln[SiH_4]} = \frac{\sum_m \frac{m}{k_m n(Si_m H_{2m+1}^-)}}{\sum_m \frac{1}{k_m n(Si_m H_{2m+1}^-)}} \equiv \overline{m} \approx m^* \qquad (3.4a)$$

$$\frac{\partial \ln J}{\partial \ln[H_2]} = -\frac{\sum_m \frac{(m-1)}{k_m n(Si_m H_{2m+1}^-)}}{\sum_m \frac{1}{k_m n(Si_m H_{2m+1}^-)}} \equiv -(\overline{m}-1) \approx -(m^*-1). \qquad (3.4b)$$

The partial derivatives signify that the concentrations of remaining presursor species, as well as temperature, are kept constant. The approximate equalities apply only in cases where there exists a critical ion-cluster size and the summations are dominated by terms near this size. m^* is the number of Si molecules in the critical ion-cluster of which m^*-1 derive from the growth species SiH_4 with the release of m^*-1 molecules of H_2. Note, however, that the true equalities of Eqs. 3.4 apply even to activationless processes with no barrier or critical cluster size. The sensitivity on seed concentration is $\partial \ln J / \partial \ln[SiH_3^-] = 1$. These results demonstrate the application of nucleation theorems to a reversible sequence of chemical reactions. Finally, Eqs. 3.4 exhibit an important general feature of nucleation theorems; namely, dependence of the isothermal rate sensitivity on reaction stoichiometry and not on local bonding condition or location (e.g., surface or interior) of species within the cluster.

4. EXTENSIONS TO BINARY AND MULTICOMPONENT NUCLEATION

The kinetic nucleation theorem is applied in this section to two models of binary nucleation for which analytic solutions can be obtained. The theorem will be demonstrated first for the Shugard-Heist-Reiss (SHR) binary nucleation model [19], which has been tested with great success through comparisons with a fully 2D kinetic model of binary nucleation in sulfuric acid-mixtures [20]. Next we present an extension of the kinetic nucleation theorem to multicomponent systems for which the thermodynamic barrier can be approximated by a quadratic free-energy surface. Finally we initiate the development of a matrix method for evaluation of $d \ln J / d \ln S$ in more complicated kinetic schemes, including multistep and multicomponent nucleation processes, for which simple analytic solutions cannot be obtained.

4.1 Application to the Shugard-Heist-Reiss model

The Shugard-Heist Reiss (SHR) model is a specialization of the full binary nucleation kinetics to the case that nucleation occurs primarily through stepwise addition to clusters of a single component (e.g. sulfuric acid), with rapid equilibration along the orthogonal coordinate (e.g. water evaporation and growth). The SHR steady-state nucleation rate takes the double summation closed form [19]:

$$J = \left\{ \sum_j \left[\sum_i \beta_a(i,j) n(i,j) \right]^{-1} \right\}^{-1} \tag{4.1a}$$

where $\beta_a(i,j) \equiv c_a s(i,j) f(0,1)/4 = c_a s(i,j) n(0,1)/4$, c_a is the mean molecular speed of an acid molecule, and $f(0,1) = n(0,1)$ is the number concentration of acid molecules in the vapor. $n(i,j)$ is the constrained equilibrium number concentration of clusters containing i molecules of water and j molecules of acid and $s(i,j)$ is the surface area of one such cluster. In the derivation of Eq. 4.1 the approximation is made that the nucleation flux occurs solely in the direction parallel to the acid (j) coordinate. Thus we could have written the overall current, instead, as a sum of noninteracting parallel currents along the j-coordinate:

$$J = \sum_i J_i = \sum_i \left(\sum_j \frac{1}{\beta_a(i,j) n(i,j)} \right)^{-1} \tag{4.1b}$$

where the inner summation has the same form as in Eq. 2.1. Although Eqs. 4.1a and 4.1b are not equivalent algebraically, they must give very nearly the same result under the condition that the flux occurs predominately along the j-coordinate.

Letting S_1 and S_2 denote the saturation ratios for water and acid, respectively, we obtain from Eq. 4.1a:

$$\frac{\partial \ln J}{\partial \ln S_2} = \frac{\sum_j (j+1) R_j}{\sum_j R_j} \equiv \sum_j (j+1) P_b(j) = 1 + \sum_j \sum_i j P_T(i,j) \approx j^* + 1 \tag{4.2a}$$

$$\frac{\partial \ln J}{\partial \ln S_1} = \frac{\sum_j \langle i \rangle_j R_j}{\sum_j R_j} = \sum_j \sum_i i P_T(i,j) \approx i^* \qquad (4.2b)$$

where $R_j \equiv [\sum_i \beta_a(i,j) n(i,j)]^{-1}$ and (i^*, j^*) is the composition at the saddle point. In Eq. 4.2b, the quantity $\langle i \rangle_j$ defines a different kind of average:

$$\langle i \rangle_j \equiv \frac{\sum_i i \beta_a(i,j) n(i,j)}{\sum_i \beta_a(i,j) n(i,j)} \equiv \sum_i i Q_b(i,j) \qquad (4.3a)$$

Equations 4.2 and 4.3 introduce the normalized distributions $P_b(j)$ and $Q_b(i,j)$, with subscript "*b*" for binary case, and the normalized product distribution $P_T(i,j) = P_b(j) Q_b(i,j)$. Another interpretation of Eq. 4.3a follows from the *j*-coordinate flux condition:

$$\langle i \rangle_j = \sum_i i Q_b(i,j) = \sum_i i Q_b(i) = \frac{\sum_i i J_i}{J} \equiv \langle i \rangle \qquad (4.3b)$$

showing that this flux condition implies that Q_b is independent of *j* and that $\langle i \rangle$ is a flux-weighted average over the water coordinate that is independent of *j*. Unlike the average of Eq. 2.8, $\langle i \rangle$ will be dominated by those clusters near the *minimum* in a slice of the binary free-energy surface having fixed acid occupation number j. The approximate equalities of Eqs. 4.2, yielding results in terms of the nucleus composition, compare favorably with Eqs. 18 and 19 of Ref. 4 derived assuming a prefactor-exponent form for the binary nucleation rate. Higher-order derivatives of $\ln J$ are obtained as flux (J_i)-weighed averages over the 1D steady-state nucleation currents as is evident from Eqs. 4.1b and 4.3b (see Appendix).

4.2 Application to a quadratic free-energy surface

The approximation that the free-energy surface is quadratic in the saddle point region presents an interesting case amenable to exact solution. Figure 3 shows a quadratic surface in the orginal cluster (i , j) coordinates and in the principal coordinates (ξ,η) centered on the critical nucleus (i^*, j^*). In principal coordinates, the surface takes the separable form:

$$\frac{W(\xi,\eta)}{kT} = \frac{W(0,0)}{kT} - a\xi^2 + b\eta^2 \tag{4.4}$$

where a and b are positive quantities, resulting in a saddle point at $\xi = \eta = 0$. The solid (hyperbolic) curves are contours of constant W for $W = W^*$, $W^* \pm kT$, and $W^* \pm 2kT$. Eq. 4.4 implies an equilibrium cluster population satisfying the Boltzmann relation, $n(i,j) = n(i^*,j^*)\exp[a\xi^2(i,j) - b\eta^2(i,j)]$.

Distribution functions similar to those introduced above for the SHR model are obtained along the reactive and orthogonal coordinates ξ and η, respectively. If one neglects the size dependence of the kinetic terms $\beta_1(i,j) = c_1 s(i,j)n(1,0)/4 \approx \beta_1$, $\beta_2(i,j) = c_2 s(i,j)n(0,1)/4 \approx \beta_2$ in the region of critical cluster size, these distributions are Gaussian and separable in the quadratic free-energy surface model. Assuming continuous size coordinates and carrying out the integrations yields the normalized distributions:

$$P_b(\xi) = \sqrt{\frac{a}{\pi}}\exp(-a\xi^2) \tag{4.5a}$$

and

$$Q_b(\eta) = \sqrt{\frac{b}{\pi}}\exp(-b\eta^2). \tag{4.5b}$$

The dashed (elliptical) contours of Fig. 3 depict the σ and 2σ surfaces (1 and 2 standard deviations, respectively) for the bivariate Gaussian distribution $P_T(\xi,\eta) = P_b(\xi)Q_b(\eta)$. The

disposition of these elliptical surfaces with respect to the critical cluster size depends only on the coefficients of bivariate products ($ii,\ jj,\ ij$) in the cluster coordinate expansion for $W(i,j)$. Specifically, the squared lengths of the principal axes, which are proportional to the principal values (variances), and orientation with respect to the original coordinate axes are independent of the gas phase species supersaturations, S_1 and S_2, as the latter appear only in the coefficients of terms linear in *i* and *j*.

Separation of variables in the principal frame (Eqs. 4.4 and 4.5) conveys special properties to the surfaces of constant $f(i,j)/n(i,j)$, where $f(i,j)$ is the steady state concentration of clusters of size (i,j). These "Φ" contours ($\Phi(i,j) = f(i,j)/n(i,j)$) have been studied for binary mixtures and show interesting tendencies toward quasi-universal behavior [21 - 23]. It is not difficult to show that two of the most significant of these tendencies, linearity and insensitivity to the activities of gas phase species, hold rigorously for a quadratic free-energy surface. Linearity follows from the separation of variables in Eqs. 4.5 resulting in an analytic solution for the gradients of Φ:

$$\nabla_{\xi}\Phi(\xi,\eta) = -P_b(\xi);\ \nabla_{\eta}\Phi(\xi,\eta) = 0, \tag{4.6}$$

subject to the boundary conditions $\Phi(\xi,\eta) = 1$ $(\Phi(\xi,\eta) = 0)$ for small (large) values of ξ. Thus the constant Φ contours (dashed lines in Fig. 3) are linear and parallel to the η axes, with $\Phi(0,0) = 1/2$ at the critical cluster size. The solution given by Eq. 4.6 is based on the factorization $P_T(\xi,\eta) = P_b(\xi)Q_b(\eta)$ and applies even when the component distributions are non-Gaussian.

Insensitivity of the Φ contours to gas phase species activity is not surprising given the preceding demonstration that the probability distributions $P_b(\xi)$ and $Q_b(\eta)$, and therefore the Φ

contours, are *independent* of supersaturation in the quadratic surface model. This insensitivity is also consistent with the vanishing of third-order cumulants for the Gaussian distribution; implying, from Eq. A6, that the variance of, for example, $P_b(\xi)$, which determines the Φ contour spacing, is independent of S_2. Superimposed on the figure is a schematic depiction of the distribution of nucleation current (arrows). The nucleation flux will in general not be orthogonal to the Φ contours as depicted in Fig. 3; but it cannot be parallel to them. Letting $J_x(i,j)$ and $J_y(i,j)$ denote the local currents in the horizontal (*i*) and vertical (*j*) directions, respectively, the full result is [21, 23]:

$$\frac{J_y(i,j)}{J_x(i,j)} = \frac{\beta_2(i,j)}{\beta_1(i,j)}\tan(\omega) \approx \frac{\beta_2}{\beta_1}\tan(\omega) \qquad (4.7)$$

where ω is the angle between the Φ gradient and the *i*-axes and the last equality applies under the approximation that the monomer addition rates are constant. Figure 3 depicts the special case that the ratio of monomer addition rates for the two species is unity.

Li and Nishioka obtained steady-state nucleation flux profiles in binary systems under the assumptions: (1) ω may be treated as constant in a local region, and (2) the Φ contours are linear [23]. The preceding analysis shows that these conditions hold rigorously for the quadratic free-energy surface. Accordingly, the analysis of Li and Nishioka carries over to this special case and their methods can be used to obtain analytic expressions for the nucleation flux profile and steady-state nucleation rate. Apart from the change to continuous variables, the resulting rate is similar to that of the SHR model, for which the Φ contours also satisfy the Li and Nishioka conditions and a double integration here, rather than summation, gives the rate. Substituting for $n(i,j)$ and integrating over the Gaussian distributions gives the exact result:

$$J = n(i^*, j^*)\sqrt{\frac{a}{b}}(\beta_2 \sin\omega + \beta_1 \cos\omega). \tag{4.8}$$

For the sensitivities we obtain:

$$\begin{aligned}
\frac{\partial \ln J}{\partial \ln S_2} &= \iint (j^* + \xi) P_T(\xi, \eta) d\xi d\eta + \frac{(\beta_2/\beta_1)\tan(\omega)}{1 + (\beta_2/\beta_1)\tan(\omega)} = j^* + \frac{(\beta_2/\beta_1)\tan(\omega)}{1 + (\beta_2/\beta_1)\tan(\omega)} \\
\frac{\partial \ln J}{\partial \ln S_1} &= \iint (i^* + \eta) P_T(\xi, \eta) d\xi d\eta + \frac{1}{1 + (\beta_2/\beta_1)\tan(\omega)} = i^* + \frac{1}{1 + (\beta_2/\beta_1)\tan(\omega)}
\end{aligned} \tag{4.9}$$

showing similar dependence on P_T as in Eqs. 4.2, but with vanishing mean values of ξ and η at the saddle point composition. For $\omega = \pi/2$, the Φ contours are oriented as in the SHR model and Eqs. 4.9 reduce to:

$$\begin{aligned}
\frac{\partial \ln J}{\partial \ln S_2} &= j^* + 1 \\
\frac{\partial \ln J}{\partial \ln S_1} &= i^*
\end{aligned}$$

showing that, apart from the distinction between continuous and discrete cluster coordinates, the approximate equalities in Eqs. 4.2 become exact for a quadratic free-energy surface. The third and higher-order derivatives vanish due to the fact that P_T is Gaussian (see Appendix). Thus for a quadratic free-energy surface, the logarithm of the nucleation rate is rigorously a quadratic function of the gas phase supersaturations $\{\ln S_i\}$. The quadratic surface model described here is readily extendable to multidimensional saddle points for systems having more than two components involved in the nucleation process.

4.3 Matrix method

For binary systems with strong deviations from ideality, the potential surfaces can be considerably more complicated [24]. Furthermore the major nucleation flux may even bypass the

saddle point completely [20, 24]. For these more complex situations a matrix method can be useful for evaluation of $d\ln J / d\ln S$. Developed in [25, 26], the approach applies both to multistep processes (i.e. to the growth of clusters through addition and subtraction of dimers, trimers and higher-order clusters, as well as monomer) and multicomponent nucleation. These processes are related under the method, which maps the multicomponent compositional grid point by point to a line, which can then be treated formally as a multistep single component process. In either case the nucleation rate can be written in the form:

$$J = (a^{\mathrm{T}} U^{-1} a)^{-1} \tag{4.10}$$

where $a^T = \{1,1,\ldots,1\}$ is the unit row vector and $U = \sum_{r=1}^{l} U^{(r)}$. Each $U^{(r)}$ contains only contributions from *r*-step transitions and factors as $U^{(r)} = [F^{(r)}]^T G^{(r)} [F^{(r)}]$ where $F^{(r)}$ is a constant rectangular lower triangular matrix having elements either zero or unity and $G^{(r)}$ is a square diagonal matrix having elements $G^{(r)}_{gg} = \beta^{(r)}_{g-r+1} n_{g-r+1}$. As $\beta^{(r)}$ is the forward rate constant for *r*-step transitions, it is proportional to n_r for a multistep single component process, or to a β_i in a multicomponent process; thus the matrix U depends only on the constrained equilibrium cluster growth rates. For a one-component and one-step process ($l = 1$), Eq. 4.10 reduces to Eq. 2.1. Equation 4.10 is a useful starting point for extending the kinetic nucleation theorem to multi-step and multi-component nucleation processes. Differentiation gives a matrix expression for $\partial \ln J / \partial \ln S_i$ where S_i is the saturation ratio of species *i* in a multicomponent system:

$$\frac{\partial \ln J}{\partial \ln S_i} = \frac{a^T [U^{-1} (\partial U / \partial \ln S_i)] U^{-1} a}{a^T U^{-1} a} = p^T (\partial U / \partial \ln S_i) U^{-1} a \tag{4.11}$$

where to calculate the derivatives of $\ln J$ we employ the identities $dJ = -J^2 dJ^{-1}$ and $dU^{-1} = -U^{-1} dU U^{-1}$. The last equality is a rewriting in terms of the column vector $p = JU^{-1}a$, which is the analogue of the probability *P(g)* in unary nucleation. From the structure of U it is readily seen that differentiation of the rhs of Eq. 4.11 reduces to differentiation of the diagonal elements of $G^{(r)}$. Returning to the single-component one-step process, U itself is diagonal, the term in brackets is $[U^{-1}(dU / d\ln S_1)]_{gg} = (g+1)$, and $(U^{-1}a)_g = 1/(\beta_g n_g)$. Thus, noting that pre-multiplication by the row vector a^T is equivalent to summation, it is seen that Eq. 4.11 reduces

to Eq. 2.7 for this special case. Differentiation of Eq. 4.11, in turn, yields the second-order rate sensitivities:

$$\frac{\partial^2 \ln J}{\partial(\ln S_i)\partial(\ln S_j)} = p^T \frac{\partial^2 U}{\partial(\ln S_i)\partial(\ln S_j)} U^{-1} a + \left(p^T \frac{\partial U}{\partial \ln S_i} U^{-1} a \right)\left(p^T \frac{\partial U}{\partial \ln S_j} U^{-1} a \right) - \left(p^T \frac{\partial U}{\partial \ln S_i} U^{-1} \frac{\partial U}{\partial \ln S_j} U^{-1} a + p^T \frac{\partial U}{\partial \ln S_j} U^{-1} \frac{\partial U}{\partial \ln S_i} U^{-1} a \right) \tag{4.12}$$

Equations 4.11 and 4.12 present a general framework for computing the sensitivity of $\ln J$ with respect to variations in the $\ln S_i$, but one that requires further development for interpretation of measurements. Further development of the matrix method and its application to KNT's for binary and multicomponent nucleation will be presented in a future publication.

SUMMARY AND DISCUSSION

In this paper we derived an exact relation for the observable sensitivities $d^n \ln J / d(\ln S)^n$ in terms of cumulants over the molecular distribution of reciprocal cluster growth rates. The case having index n=1 is the usual nucleation theorem and the case n=2 wa shown to provide an interesting molecular-level reformulation of the Kelvin relation. These results apply under conditions that the law of mass action and detailed balance are maintained. In particular, the clusters must be noninteracting for the law of mass action to be valid. A significant finding is that measurements of $d^n \ln J / d(\ln S)^n$ reflect the properties of a distribution of clusters near critical size and not those of a single cluster, as the more approxiate forms of the nucleation theorem described in Sec. 1 would suggest. A similar result applies to the temperature derivative, demonstrating that $d \ln J / dT$ also depends on a weighted average of cluster energies for clusters near critical size. Extensions of the kinetic nucleation theorem were obtained for binary and multicomponent nucleation under the assumption that the multivariate cluster free-energy surface has quadratic form and for a class of binary nucleation systems, such as sulfuric acid-water mixtures, for which the SHR model [19] is a valid approximation. Finally we initiated the development of a matrix method for computation of $d \ln J / d \ln S$ for cases involving more

complicated kinetic schemes, including multistep and multicomponent nucleation processes, for which simple analytic solutions cannot be obtained.

Inspection of the kinetic nucleation theorem suggests a number of distinctions from thermodynamic result (Eq. 1.4). First, the unit term appearing in Eq. 2.7 arises naturally from the law of mass action (cf. Eq. 2.5). Consistency of Eq. 1.4 with mass action, on the other hand, requires $d\ln J_0 / d\ln S = 1$, and for this result it was necessary to employ both the prefactor-exponent form of Eq. 1.2 and the prefactor correction of Courtney. The present derivation has been achieved without any requirements placed on either the cluster formation energy $W(g)$ or the kinetic prefactor J_0. The expression for J on which the present derivation is based, Eq. 2.1, is obtained under assumed removal of clusters beyond a certain maximum size and a steady-state current [12]; however no barrier need be present. Thus the resulting equality of 2.7 applies, for example, to the activationless monomer addition processes $A_1 + A_1 \rightarrow A_2 + A_1 \rightarrow A_3 + \cdots$ even with no barrier or critical cluster size. In the limit that the forward rate strongly dominates, $\bar{g} \cong 1$ and $d\ln J / d\ln S_1 \cong 2$, which is the expected result from chemical kinetics. The thermodynamic result, Eq. 1.4, on the other hand is more limited as it is derived under the presumption that there is a critical cluster size controlling the rate, which is of course problematic when there is no relative maximum in the free-energy of cluster formation. Finally the appearance in Eq. 2.7 of g^* (instead of Δg^*) is a consequence of assuming an ideal cluster mixture consistent with the law of mass action.

ACKNOWLEDGMENTS

Work at BNL was supported by NASA through interagency agreement number W-18,429 as part of its interdisciplinary research program on tropospheric aerosols. Work at Yale was supported by NASA Microgravity Materials Research Program, grant no. NAG8-1461, and by a junior faculty fellowship.

REFERENCES

1. D. Kashchiev, J. Chem. Phys. **76**, 5098 (1982).
2. D. W. Oxtoby and D. Kashchiev, J. Chem. Phys. **100**, 7665 (1994).
3. Y. Viisanen, R. Strey, and H. Reiss, J. Chem. Phys. **99**, 4680 (1993).
4. R. Strey and Y. Viisanen, J. Chem Phys. **99**, 4693 (1993).
5. R. McGraw and A. Laaksonen, Phys. Rev. Letts. **76**, 2754 (1996).
6. R. K. Bowles, R. McGraw, P. Schaaf, B. Senger, J. -C. Voegel, and H. Reiss, J. Chem. Phys. **113**, 4524 (2000).
7. R. K. Bowles, D. Reguera, Y. Djikaev, and H. Reiss, J. Chem. Phys. **115**, 1853 (2001).
8. I. J. Ford, J. Chem. Phys. **105**, 8324 (1996).
9. Use of the relative rate sensitivity often leads to reduction of complex chemical kinetic expressions to simpler and more insightful form. For an interesting application to the rates of ozone production in the atmosphere see: L. Kleinman et al., Geophysical Res. Letts. **24**, 2299 (1997).
10. W. G. Courtney, J. Chem. Phys. **35**, 2249 (1961).
11. I. J. Ford, Phys. Rev. **E56**, 5615 (1997).
12. F. F. Abraham, *Homogeneous Nucleation Theory* (Academic, New York, 1974) chapt. 5.
13. W. J. Moore, *Physical Chemistry*, (Prentice-Hall, Englewood Cliffs, 1962) chapt. 6.
14. M. Abramowitz, and I. A. Stegun, *Handbook of Mathematical Functions* (Dover, New York, 1972) pp. 928-930.
15. J. Wölk, and R. Strey, J. Phys. Chem. **B105**, 11683 (2001).
16. R. Strey, P. E. Wagner., and T. Schmeling, J. Chem. Phys. 84, 2325 (1986).

17. R. McGraw, in *Nucleation and Atmospheric Aerosols 2000, 15 th International Conference Rolla, Missouri 2000,* AIP Conference Proceedings Vol. 534, Eds. B. N. Hale and M. Kulmala (AIP, New York, 2000) pg. 373.
18. S. L. Girshick, J. Chem. Phys. **107**, 1948 (1997).
19. W. J. Shugard, R. H. Heist, and H. Reiss, J. Chem. Phys. **61**, 5298 (1974).
20. R. McGraw, J. Chem. Phys. **102**, 2098 (1995).
21. B. E. Wyslouzil and G. Wilemski, J. Chem.Phys. **110**, 1202 (1999).
22. B. E. Wyslouzil and G. Wilemski, J. Chem.Phys. **105**, 1090 (1996).
23. J. S. Li and K. Nishioka, Chem. Phys. Lett. **295**, 211 (1998).
24. B. E. Wyslouzil and G. Wilemski, J. Chem.Phys. **108**, 1137 (1995).
25. D. T. Wu, J. Chem. Phys. **97**, 1922 (1992).
26. D. T. Wu, *Nucleation Theory*, in Solid State Physics, **Vol. 50**, 37 (1997).

FIGURE CAPTIONS

Figure 1. Homogeneous nucleation of water vapor. Data points are measurements at T=250K from Table 2 of Wölk and Strey [15]. Superimposed on these measurements are best fits to the data using Taylor expansion about the reference point $S_0 = 10$, indicated by the intersection of the horizontal and vertical gray lines (see Eq. 2.9b). Truncating the expansion after the linear term produces the dashed line fit and the first cumulant, $\kappa_1 = 29.86$. Truncation after the quadratic term produces the solid curve fit and the second cumulant, $\kappa_2 = 49.42$. See text for the comparison of these model-free results with the predictions of classical nucleation theory.

Figure 2. Top: nucleation barrier obtained using the capillary drop model from classical nucleation theory. Results for the homogeneous nucleation of water vapor at $250K$ and reference supersaturation from Fig. 1, $S = 10$. Bottom: corresponding normalized distributions; solid curve, $P(g)$ from Eq. 2.8; dotted curve, the normalized $1/n_g$ distribution discussed below Eq. 2.10.

Figure 3. Quadratic free-energy surfacefor a binary mixure showing contours (solid curves) for W^*, $W^* \pm kT$, and $W^* \pm 2kT$. The principal coordinate axes ξ and η are indicated and lines of constant Φ (dashed lines and Φ values) are also shown. Superimposed on the figure is a schematic depiction of the distribution of nucleation current (arrows) for the case that the ratio of monomer addition rates for the two species is unity. See text for explanation of the elliptical probability curves.

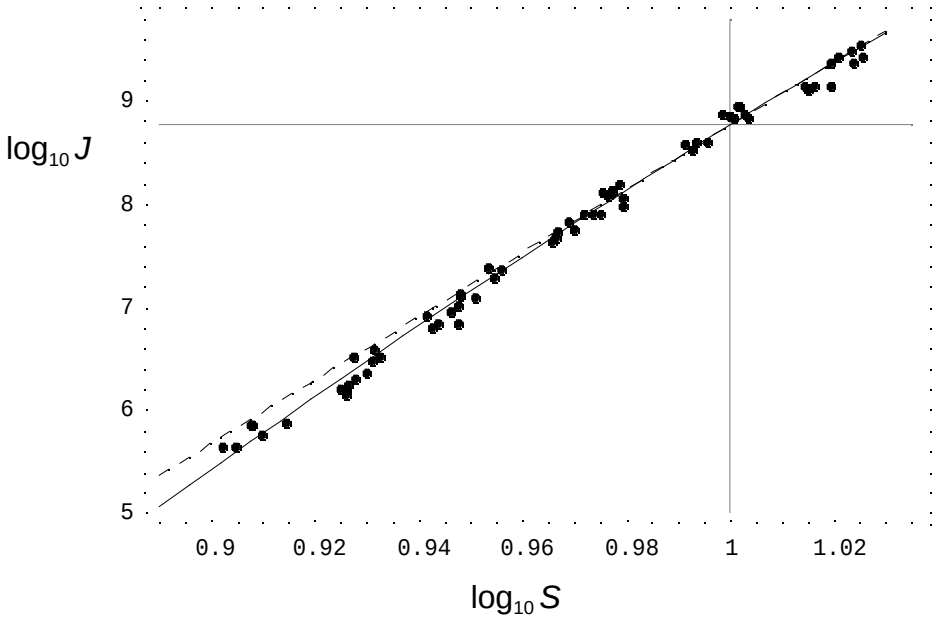

Figure 1

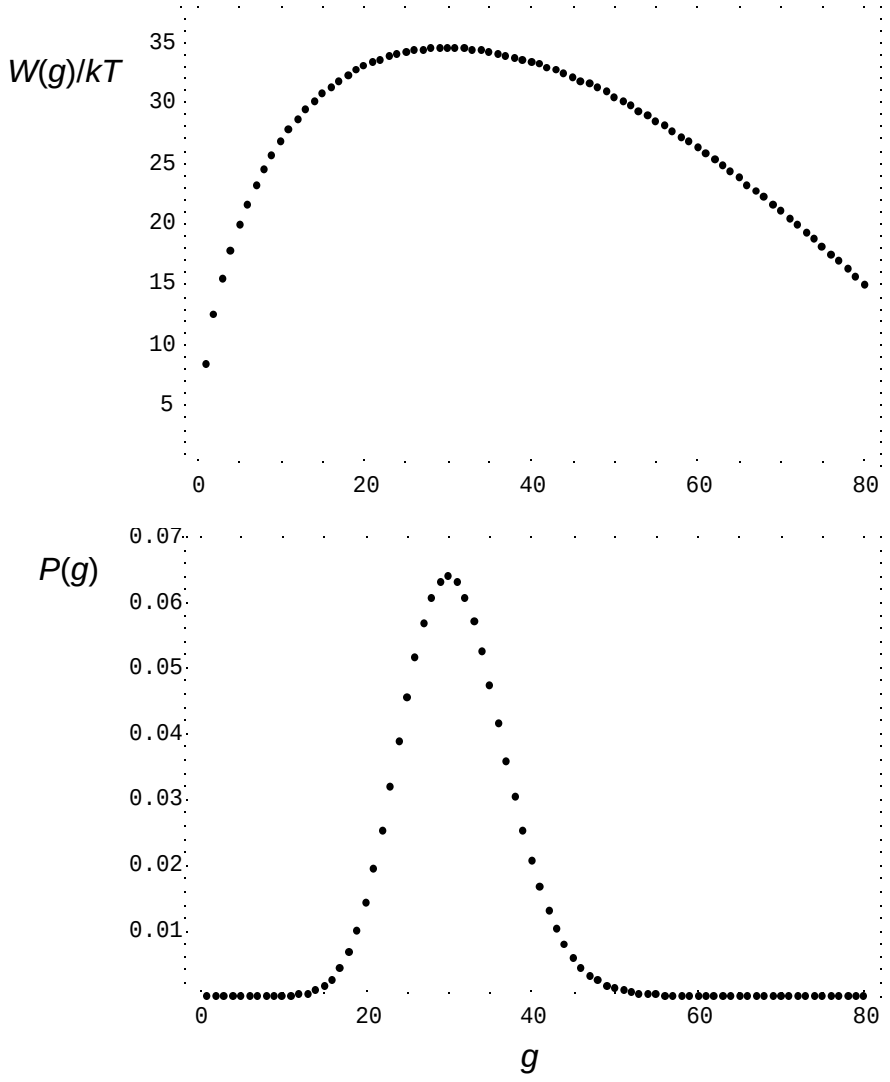
W(g)/kT
35
30
25
20
15
10
5
0
20
40
60
80
P(g)
0.07
0.06
0.05
0.04
0.03
0.02
0.01
0
20
40
60
80
g

Figure 2

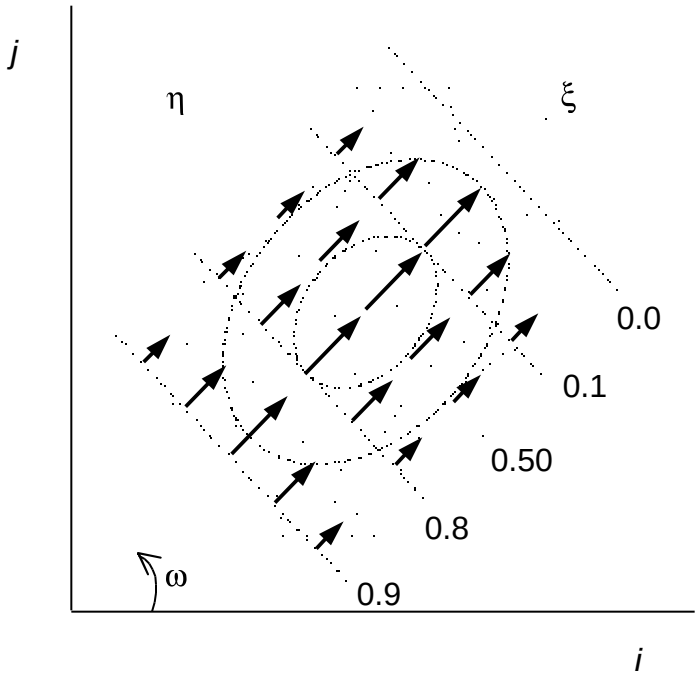

Figure 3